Multifrequency Radar Imagery and Characterization of Hazardous and Noxious Substances at Sea

Sébastien Angelliaume[(1)], Brent Minchew [(2)], Sophie Chataing [(3)]
Philippe Martineau[(1)] and Véronique Miegebielle[(4)]
[(1)] ONERA, France, [(2)] BAS, United Kingdom, [(3)] CEDRE, France, [(4)] TOTAL, France
Sebastien.Angelliaume@onera.fr

Abstract

The increase in maritime traffic, and particularly the transport of chemical products, necessitates enhancement of methods of prevention and intervention towards the spills of chemicals in the environment. Maritime pollution by chemical products occurs at much lower frequency than spills of oil, however the consequences of a chemical spill can be more wide-reaching than those of oil. While detection and characterization of hydrocarbons have been the subject of numerous studies, detection of other chemical products at sea using remote sensing has been little studied and is still an open subject of research. To address this knowledge gap, an experiment was conducted in May 2015 over the Mediterranean Sea during which controlled releases of hazardous and noxious substances were imaged by remote sensing systems. The aim of these experiments and subsequent analysis is to establish a procedure for collecting evidence of illegal maritime pollution by noxious liquid substances using airborne sensors.

In this paper we discuss the experimental procedure, which was carried out in collaboration with the French Navy and Customs, and report the main results from the airborne radar imaging campaign. We develop an accurate method for using multifrequency radar sensors to detect and quantify impact of chemical products at sea. We conclude by demonstrating the capability of radar imagery to distinguish two different substances within the same spill.

1 Introduction

Airborne and spaceborne radar remote sensing is often used for oil slick detection over maritime surface (Brekke and Solberg, 2005; Girard-Ardhuin et al., 2005; Garcia-Pineda et al., 2009; Solberg 2012). In the oil and gas sector, oil slick detection using remote sensing is of great interest for exploration and environment program domains. In an operational context, oil slicks are usually detected using airborne and/or spaceborne synthetic aperture radar (SAR). Indeed, the oil layer on top of the sea surface damps the so-called "capillarity waves", which are the origin of the sea surface roughness that significantly contributes to backscattered signal at high frequency (microwave domain). Once detected, the spill is characterized using optical imagery (Leifer et al., 2012).

Unlike hydrocarbons, there is limited research on the detectability of Hazardous and Noxious Substances (HNS) at sea using remote sensing. In that context, an experimental campaign of measurements (called POLLUPROOF) was conducted in May 2015 in the Mediterranean Sea (off the French coast). Controlled release of six chemical and non-hydrocarbon oil products were carried out in collaboration with the French Navy and Customs. Polarimetric SAR (POLSAR) data were acquired at X- (9.75 GHz) and L-band (1.325 GHz) simultaneously by SETHI, the ONERA airborne SAR system (Bonin et al., 2009), over released products. Hyperspectral data (SWIR and LWIR) have also been acquired by ONERA and RDDC; French customs have also participated to the exercise at sea with their airborne surveillance

Angelliaume, S., B. Minchew, S. Chataing, Ph. Martineau, and V. Miegebielle, Multifrequency Radar Imagery and Characterization of Hazardous and Noxious Substances at Sea, Proceedings of the Thirty-ninth AMOP Technical Seminar, Environment and Climate Change Canada, Ottawa, ON, pp. 364-382, 2016.

system (X-band RAR, IR and UV imagery); but RAR (Real Aperture Radar) and optical remote sensing is beyond the scope of this paper.

The aim of this work is first to study the capability of high resolution multifrequency SAR imagery to detect HNS at sea and then to study the potential of radar imagery to quantify and characterize the spill: thickness or amount of product and distinction between different products.

This paper is organized as follows: Section 2 describes the experimental measurement campaign at sea; Section 3 presents the methodology for detecting and characterizing HNS; Section 4 presents some original results and demonstrates the relevance of radar imagery for monitoring non-hydrocarbon pollution over maritime surface.

2 Experimentation at Sea

2.1 Radar Imagery

SETHI is the airborne remote sensing imaging system developed by ONERA, (Bonin et al., 2009). It integrates a new generation of radar and optronic payloads. It can operate over a wide range of frequency bands from UHF-VHF, to X-band including L-band with long range, very high resolution, polarimetric and interferometric capabilities. SETHI is a pod-based system operating onboard a Falcon 20 Dassault aircraft which is the property of the AvDEF company. For the POLLUPROOF campaign, quad-pol SAR data have been acquired simultaneously at X- and L-band, with a resolution of 0.5 and 1.0 m, respectively. Images are generated with an azimuth resolution equal to the range resolution at both X- and L-band, which implies an integration time equal to 1.1 s at X-band and 4.1 s at L-band. Main characteristics of acquisition are summarized in Table 1.

Table 1 SETHI - Waveform.

Frequency	Bandwith	Polarization	Incidence angle	Swath
X	300 MHz (9.6-9.9 GHz)	Quad-pol (HH, HV, VH, VV)	45° (34-52°)	1500m (slant range)
L	150 MHz (1.25-1.4 GHz)	Quad-pol (HH, HV, VH, VV)	45° (34-52°)	1500m (slant range)

Incidence angle varies across the swath from 34° to 52°. Instrumental noise floor has been estimated using the method proposed in (Hajnsek et al., 2012) and the results are shown Figure 1. The Noise Equivalent Sigma^0 (NESZ) is very low, allowing sufficient Signal to Noise Ratio over the spill for efficient analysis.

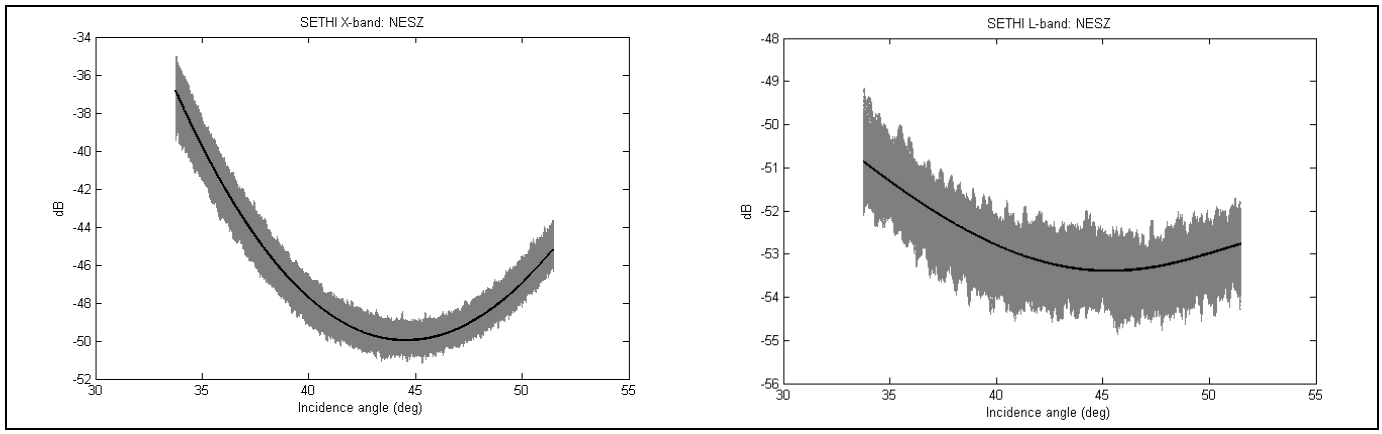

Figure 1 SETHI - Instrumental noise at X-band (left) and L-band (right).

2.2 Chemical Products

Six chemical substances have been chosen to evaluate the capability of remote sensing sensors. The choice was made to cover different chemical families and be as representative as possible of chemical products often transported by sea and classified as noxious substances. The chemical substances selected are the following:

- Category I : vegetal oil and fatty acid esters
  - Rapeseed/colza oil
  - Fatty Acid Methyl Esters (FAME)
- Category II : petrochemical products
  - Toluene
  - Heptane
  - Xylene
- Category III : alcohols and derivatives
  - Methanol

Toluene: Toluene, also named methylbenzene or phenylmethane is an aromatic hydrocarbon. This product is commonly used as chemical reagent or solvent, particularly in the industrial sector. Toluene is a colorless liquid at ambient pressure and temperature, with a specific gravity of 0.867 $g.cm^{-3}$. Toluene is nearly insoluble in water (0.535 $g.L^{-1}$ at 25 °C) and tends to evaporate relatively easily (vapor pressure of 2.91 kPa at 20 °C). Toluene vapors are 3.1 times heavier than air and are preferentially located next to the ground.

Heptane: Heptane is the generic term to identify one of the 9 isomers of C_7H_{16} and is a saturated hydrocarbon of the linear alkane family. This is a constituent of fuel and is used as extraction solvent, synthesis intermediate in chemical industry and as solvent for glues, inks, rubbers and plastics. At ambient pressure and temperature, heptane is a colorless liquid, volatile (6 to 7.7 kPa at 20 °C) and nearly insoluble in water (< 2 $mg.L^{-1}$). With a specific gravity of 0.710 $g.cm^{-3}$, heptane is lighter than water and floats.

FAME: Fatty Acid Methyl Esters are biofuel directly added in conventional fuels such as diesel. At ambient pressure and temperature, they are a liquid with a specific gravity of

0.888g.cm^{-3}. This product is pretty much insoluble in water (solubility of 0.023mg.L^{-1} at 20°C) and practically does not evaporate (vapor pressure of 0.42kPa at 25°C).

Methanol: Methyl alcohol or methanol is the simplest alcohol of chemical formula CH_3OH. This is a colorless light liquid (specific gravity of 0.791 g.cm^{-3}), volatile (vapor pressure of 12.3 kPa at 20 °C), miscible in water, inflammable and toxic with a characteristic odor. At ambient temperature, this polar liquid is used as antifreeze (for coolant for example), solvent or fuel (in aeromodelling for example). Methanol is not present in large amounts in nature and is industrially produced. Methanol is mainly used as basic material for chemical synthesis of more complex chemical products. Nearly 40 % of methanol is converted in formaldehyde to be then transformed in plastics, synthetic resins, paints, explosives or fabrics.

Rapeseed Oil: Rapeseed or colza oil is a vegetal oil obtained from colza seeds crushing. This is the second most consumed food oil in France after sunflower oil. At ambient pressure and temperature, rapeseed oil is a viscous yellowish liquid with a specific gravity of 0.910 g.cm^{-3}. Rapeseed oil is insoluble in water and does not evaporate (vapor pressure below 0.01 kPa at 25 °C).

Xylene: Xylene or dimethylbenzene is a group of aromatic hydrocarbons with one methyl derivative on benzene. It is naturally present in oil, xylene is observed in (diesel) engine exhaust gases, either a residual oil chemical or formed during incomplete combustion. Xylene is also produced from oil in the petrochemical industry and is one of the 30 most produced chemicals in the USA. It is used in the printing industry, rubber and leather industries mainly as a solvent. Xylene is a colorless and very inflammable liquid with a pleasant fragrance. Chemical properties are similar from one isomer to another. Its specific gravity of 0.87 g.cm^{-3} makes it float on water. Xylene is slightly soluble in water (solubility below 20 mg.L^{-1}) and is not likely to evaporate (vapor pressure of 0.89 kPa at 20 °C). Xylene vapors are heavier than air and tend to locate next to the ground.

These chemicals are part of the most transported substances by maritime transport in Europe and some of them are classified as the most noxious substances in the IBC Code (IMO). During the POLLUPROOF experiment, 1 m^3 of each of these six products was released at sea and imaged by airborne remote sensing sensors.

2.3 Planning of Measurements

Experimentation took place in May 2015. Three flights were performed, with two releases per flight:

- **First flight** took place on the 18th of May, from 16:40 to 17:30 UTC. The sea was calm. Heptane and toluene were released from 2 semi-submersible 1 m^3 tanks at 16:30 and 16:35 UTC, respectively (Figure 2). Heptane and toluene were released at a fixed position (separated by about 100 m); SAR acquisitions began 10 min after the first release (heptane) and 5 min after the second release (toluene).
- **Second flight** took place on the 22nd of May, from 13:25 to 13:55 UTC. There was a heavy swell, restricting any activity at sea; hence products were released directly from the back of the boat (French Navy) advancing towards the east at a speed of 1 knot: methanol was released from 12:35 to 12:45 UTC and xylene from 12:55 to 13:25 UTC (Figure 3). SAR acquisitions began 40 min after the end of the first release (methanol) and at the end of the second release (xylene).

- **Third flight** took place on the 22nd of May, from 15:20 to 16:50 UTC. Because of the swell, products were also released directly from the back of the boat advancing towards the east at a speed of 1 knot: rapeseed oil was released from 15:00 to 15:30 UTC and FAME from 15:25 to 15:40 UTC (Figure 4). SAR acquisitions were synchronized with the release.

Sea and weather conditions during experimentation are described in Table 2 below.

Table 2 Environmental conditions during experimentation at sea.

Date	Time (UTC)	Wind (from)		Wave (from)	
		Speed (m/s)	Direction (deg)	Height (m)	Direction (deg)
18 May, 2015	17:00	8	255	0.5	240
22 May, 2015	13:00	7	315	2	270
22 May, 2015	16:00	7	315	1.75	270

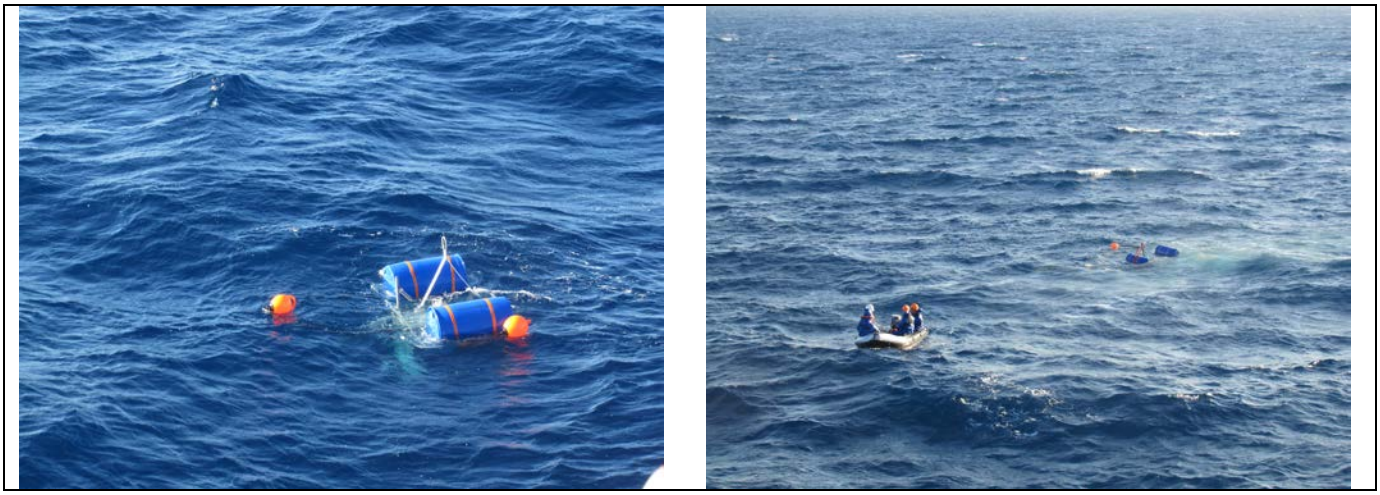

Figure 2 First flight: heptane and toluene release from semi-submersible tank.

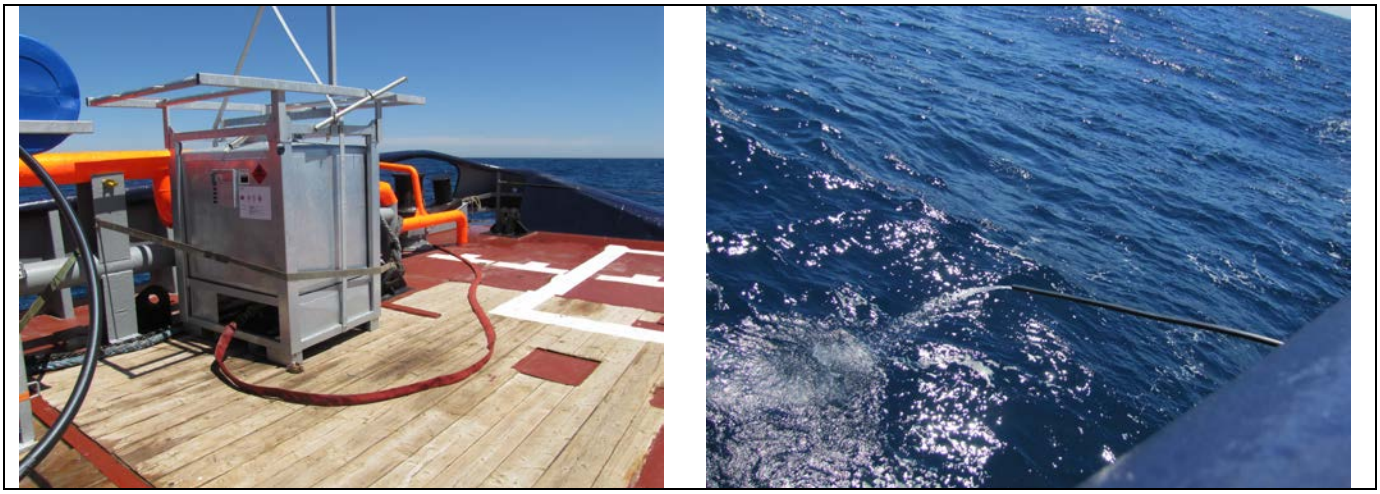

Figure 3 Second flight: methanol and xylene release from the boat.

Figure 4 Third flight: rapeseed oil (left) and FAME (right) release from the boat.

3 Methodology

3.1 Scattering from Ocean Surface

For the frequency bands mainly used in Earth Observation (X-, C- and L-band) and for incidence angles ranging from 30° to 60°, an ocean surface is a randomly rough surface where the radar backscatter is dominated by the Bragg scattering mechanism. As a consequence, the radar backscattered power, which is commonly defined by the normalized radar cross-section (NRCS), is greater in VV polarization than in HH and HV (e.g. Valenzuela, 1978). For each polarization, the NRCS is proportional to the spectral energy density of the sea surface waves with wavelength (λ_{sea}) that satisfies:

$$\lambda_{sea} = \frac{\lambda_{EM}}{2\sin(\theta_i)} \quad (1)$$

where λ_{EM} and θ_i are the wavelength and the local incidence angle of the electromagnetic (EM) waves transmitted by the radar system, respectively. Ocean wavelengths corresponding to the Bragg wavelength are shown in Figure 5 for the three most common frequency bands (X-, C- and L-band). It is obvious that the carrier frequency has a crucial impact and using different data acquired at different frequencies over the same area can provide additional information and improve our ability to characterize the imaged surface. While X- and C-band are relatively close, we can assume that the use of X- and L-band shall allow to obtain simultaneous information on different scales of the sea.

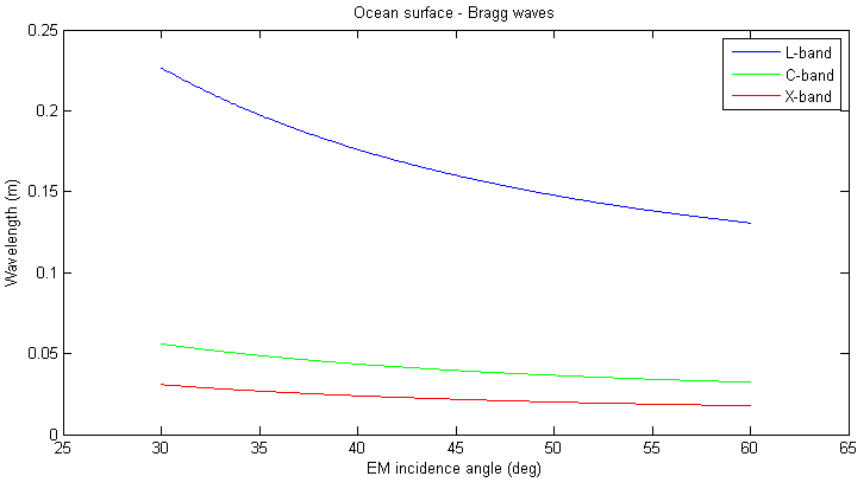

Figure 5 Ocean waves in resonance with the EM signal (Bragg mechanism).

Ocean surface is usually modeled as a composition of slightly rough tilted facets, each of which has superimposed small-scale surface roughness that creates a Bragg scatterer. Small-scale roughness is randomly distributed on the scattering surface and responds to the strength of local wind (i.e, gravity-capillarity waves). The tilt of the facet is caused by larger scale gravity waves on the ocean surface. The orientation of the facet normal in the radar reference frame is defined by two angles ψ and ξ. The resulting local incidence angle of the EM wave is:

$$\theta_i = \cos^{-1}\left[\cos(\theta + \psi)\cos\xi\right] \tag{2}$$

where θ is the EM angle of incidence relative to local, un-tilted up.

Following this approach, the sea may be modeled as the superposition of two independent processes describing the small and large scale components. Two-Scales Model (TSM), based on a spectral description of the sea surface, has been proposed to formulate this composite-surface scattering (Elfouhaily et al., 1997; Soriano and Guérin, 2008). The NRCS is then given by (Valenzuela, 1978):

$$\sigma^0_{pp} = 4\pi k^4_{EM} \cos^4\theta_i \Gamma_{pp} W \tag{3}$$

where the subscript *p* denotes either H or V polarization, $k_{EM} = 2\pi/\lambda_{EM}$ is the EM wavenumber, *W* is the spectral density of the ocean surface roughness and Γ_{pp} is the reflectivity defined by:

$$\Gamma_{pp} = \left| \left(\frac{\sin(\theta+\psi)\cos\xi}{\sin\theta_i} \right)^2 \alpha_{pp} + \left(\frac{\sin\xi}{\sin\theta_i} \right)^2 \alpha_{qq} \right|^2 \tag{4}$$

where the subscript q $(q \neq p)$ denotes either H or V polarization. The reflectivity depends on the facet tilt, the EM wave incidence angle and the scattering coefficients such that (Valenzuela, 1978):

$$\alpha_{HH} = \frac{\cos\theta_i - \sqrt{\varepsilon - \sin^2\theta_i}}{\cos\theta_i + \sqrt{\varepsilon - \sin^2\theta_i}} \quad (5)$$

$$\alpha_{VV} = \frac{(\varepsilon - 1)\left(\sin^2\theta_i - \varepsilon\left(1 + \sin^2\theta_i\right)\right)}{\left(\varepsilon\cos\theta_i + \sqrt{\varepsilon - \sin^2\theta_i}\right)^2} \quad (6)$$

The Bragg scattering coefficients only depend on the local incidence angle of the EM wave θ_i and the relative dielectric constant ε. Finally, for a given geometry of acquisition (fixed incidence angle) and assuming that the ocean surface is homogeneous over a sufficiently large area, the NRCS is only depending on the EM wavelength, the relative dielectric constant and the sea surface roughness.

In the case of an ocean surface covered by slicks, the product surface layer will dampen the capillarity waves, thereby attenuating the radar backscattered power by diminishing the surface roughness. The relative dielectric constant can also be modified in the case of a product which mixes with sea water. The resulting dielectric constant will be smaller than for pure sea water, because the relative dielectric constant of HNS is low compared to sea water (Minchew, 2012). The resulting NRCS will be lower for a product which mixes with water than for clean sea surface.

The starting point of this study is based on the assumption that in the case of a thin layer, only the short capillarity waves will be damped; when the layer gets thicker, longer capillarity waves will also be damped. These phenomena should be observable in the case of multifrequency SAR data acquired simultaneously over the same surface. Moreover, this should be enhanced when using EM wavelengths sufficiently apart (for instance X- and L-band radar frequencies) since the EM signal will simultaneously interact with hydrodynamic mechanisms of different scales (Figure 5).

3.2 Detection and Relative Quantification

Many studies have suggested using polarimetric SAR (POLSAR) parameters to improve slicks detection capability (see review by Solberg, 2012). A comprehensive comparison of those parameters was undertaken by (Angelliaume et al., 2015). Following (Kudryatsev et al., 2013), (Angelliaume et al., 2015) quantitatively demonstrates the effectiveness of the *Polarization Difference* (PD=VV-HH in linear units) for slick detection on the ocean surface. The interest to use this parameter for a marine pollutant detection application is that PD is essentially proportional to the wave number spectrum taken at the Bragg frequency (Guérin et al., 2010). It is therefore very sensitive to small scale features of the ocean surface (damped by the slick) and quite insensitive to the larger scales, which rather drive the unpolarized contribution to the NRCS.

The main drawback of the *Polarization Difference (PD)* is that it is not normalized, making it difficult to define a threshold with which a detection map can be established. To overcome this limitation, we propose a normalized variant of PD. We note that PD ranges from a maximum value (PD_{max}) that occurs in the case of a clean sea surface and goes to 0 as the impact of the substance on the surface increases, since both VV and HH reflectivity tend to 0 over a perfectly smooth surface. Hence, we define the *Normalized Polarization Difference (NPD)* as:

$$NPD = \frac{PD_{\max} - PD}{PD_{\max}} \qquad 0 \le NPD \le 1 \tag{7}$$

NPD is equal to 0 in the case of a clean sea surface and goes to 1 as the impact of the substance on the ocean surface increases. PD_{max} is the polarization difference value in the case of a clean sea surface and can be estimated through a physical two-scale model (Soriano and Guérin, 2008; Angelliaume et al., 2014) or an empirical model (Gregers-Hansen and Mittal, 2012), using wind speed and wind direction information.
NPD can be interpreted as an indication of the presence and the impact of a substance on the ocean surface. It can be used directly or thresholded to produce a binary detection map.

3.3 Oil/Water Mixing Index

The basic premise of the oil/water mixing index (M_{dex}) is that radar backscattered power is diminished by oil slicks through mechanical damping of Bragg-wavelength capillary waves and reductions in the relative dielectric constant of the upper few centimeters near the sea surface (Minchew et al., 2012; Minchew, 2012). By decoupling the relative contribution to signal attenuation of surface waves mechanical damping and changes in dielectric constant, we can define the characteristics of the slick along a spectrum ranging from thin surface films to thicker emulsions. This information is critical for efficient cleanup operations.

In addition to the assumptions underlying the NRCS model, Eq.(3), the process of decoupling the mechanical and electromagnetic attenuation mechanisms requires us to assume that: (1) the long-wavelength tilting of the sea surface (as described by angles ψ and ζ in Eq. (2)) is unaffected by the presence of an oil slick and (2) the dielectric constant of uncontaminated seawater is well-constrained. These assumptions allow for inferences of the long-wavelength tilting of the sea surface over the entire radar image (so long as the radar images ample areas of uncontaminated water), the dielectric constant of contaminated water, and the small-scale roughness spectrum of both contaminated and uncontaminated water. As described by (Minchew, 2012), the salient parts of the process of decoupling the mechanical and electromagnetic attenuation mechanisms can be summarized as follows:

1. Use the co-polarized ratio over uncontaminated seawater and an assumed value for the dielectric constant of pure seawater, ε_r^{water}, to infer the long-wavelength tilting of the ocean surface.
2. Calculate the short-wavelength roughness spectrum over uncontaminated water, W^{water}, by applying the tilt angles inferred in Step 1.
3. For each pixel of contaminated water, infer the local (effective) relative dielectric constant, ε_r^{oil}, from the co-polarized ratio and the inferred long-wavelength tilt angles deduced from Step 1.
4. Calculate the short-wavelength roughness spectrum over contaminated water, W^{oil}, using the dielectric constant inferred in Step 3 and the tilt angles obtained in Step 1.

M_{dex} values can then be calculated as follows:

$$M_{dex} = M_W - M_\alpha \tag{8}$$

$$M_W = \frac{W^{water} - W^{oil}}{W^{water}} \tag{9}$$

$$M_{\alpha} = \frac{|\alpha_{VV}^{water}|^2 - |\alpha_{VV}^{oil}|^2}{|\alpha_{VV}^{water}|^2} \quad (10)$$

M_W is the *normalized damping factor* and M_α is the *normalized power attenuation factor*, both are ranging from 0 to 1. M_W is a measure of how much the product will attenuate the sea surface roughness (0=no damping ; 1=total damping); M_α is a measure of how much the backscattered signal is attenuated due to a decrease of the relative dielectric constant (0=no attenuation ; 1=total attenuation). M_{dex} is ranging from -1 to 1. Negative values indicate that the decreasing of the EM signal due to the presence of HNS on the ocean is more due to a decrease of the relative dielectric constant than to a decrease of the surface roughness; meaning that the product is mixed with the sea water. On the opposite, positive values indicate that the decreasing of the EM signal is mainly due to a smoothing of the ocean surface and thus we are in presence of a product that forms a film (more or less homogeneous) on the top of the sea surface. In an operational context, this information may be valuable to identify the behavior of the HNS and guide actions to achieve.

4 Results and Discussion

4.1 Observation of Hazardous and Noxious Substances at Sea

Heptane and Toluene: Both substances were never observed in SAR images, at X- and L-band; most likely because they are extremely volatile products, which do not impact the surface roughness. Remember that products (1 m^3 each) have been released only 5 and 10 minutes before acquisitions.

Methanol and Xylene: As methanol is an extremely volatile substance soluble in the water column and as SAR acquisition began 40 min after the end of the release, methanol was never observed in SAR images. On the other side, the impact of xylene is clearly observable on X- and L-band SAR imagery, without obvious influence of the flight trajectory relative to the wind. Figure 6 shows illustrations of X-band VV polarization images acquired over xylene for upwind and crosswind observation. The size of the spill is about 1750 m x 200 m; the bright point just at the end of the spill is the ship (53 m length) from which releases were performed.

Rapeseed Oil and FAME: FAME and rapeseed oil are two persistent substances; which are both clearly observable on SAR images acquired at X- and L-band during the 3rd flight. Figure 7 shows an illustration of VV polarized images acquired simultaneously at X- and L-band over the spill at 16:07 UTC. Rapeseed oil, having been released first, corresponds to the right part of the spill; FAME is on the left. From in situ information, we know that FAME is ranging from azimuth 4100 m to 5500 m, and that rapeseed oil is from azimuth 6000 m to 8500 m, and between we have a mixture of the two products. While it is not possible to visually distinguish the FAME and rapeseed oil, we observe a significant difference between L- and X-band acquisitions. Contrast between the spill and the clean sea surface is more significant at X-band than at L-band. Figure 8 shows an azimuth profile calculated by averaging from 3800 m to 3900 m in range (the spill is between azimuth 4800 to 5600 m and azimuth 6500 to 8200 m). While at X-band the spill seems homogeneous (Figure 7 top), at L-band (Figure 7 bottom) we observe strong variation of the EM signal into the spill with dark patches, due to a stronger impact of the HNS on the sea surface roughness at wavelengths corresponding to the L-band Bragg wavelength. This observation is particularly important: as previously demonstrated by (Wismann et al., 1998) or (Gade et al., 1998), it confirms that the EM signal backscattered by HNS is

dependent on the wavelength and using different frequency bands should allow us to better characterize the spill.

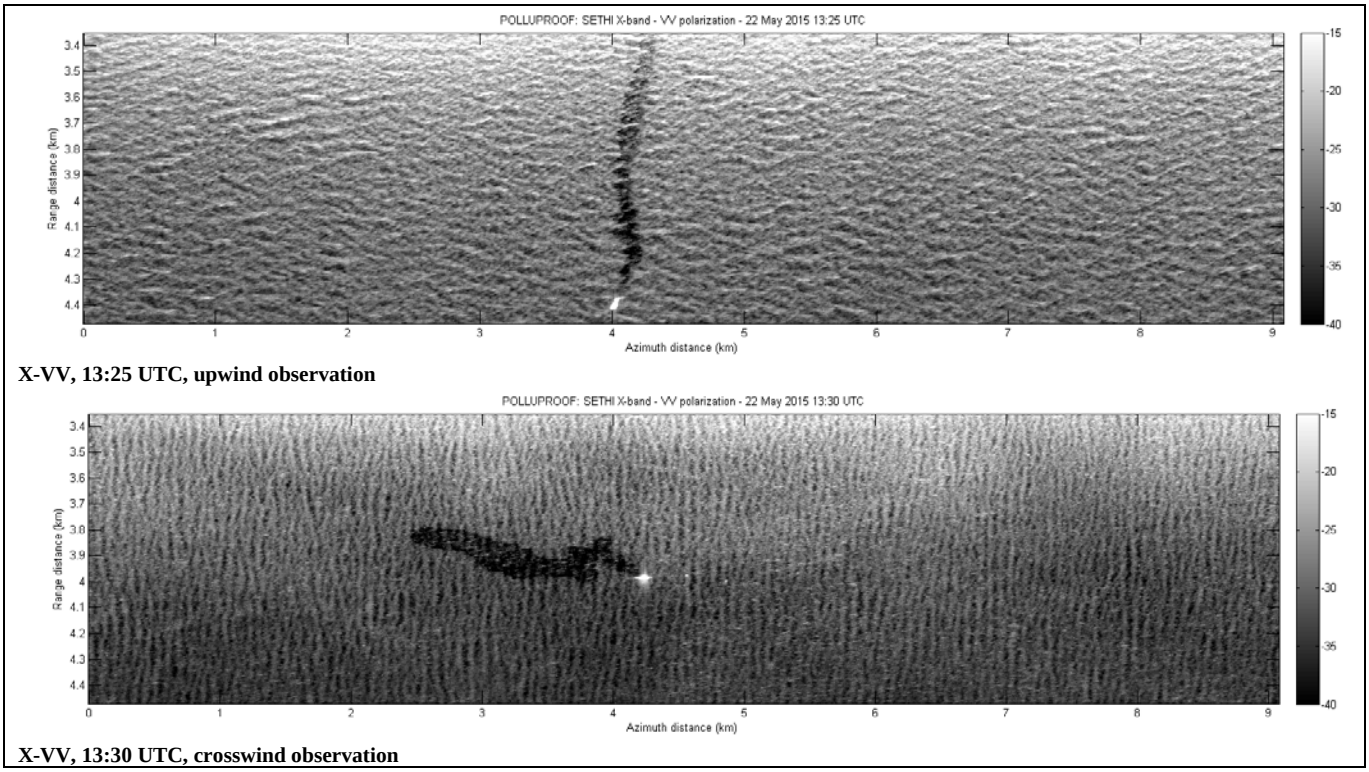

Figure 6 X-VV SAR images over xylene - upwind 13:25 UTC (top) and crosswind 13:30 UTC (bottom).

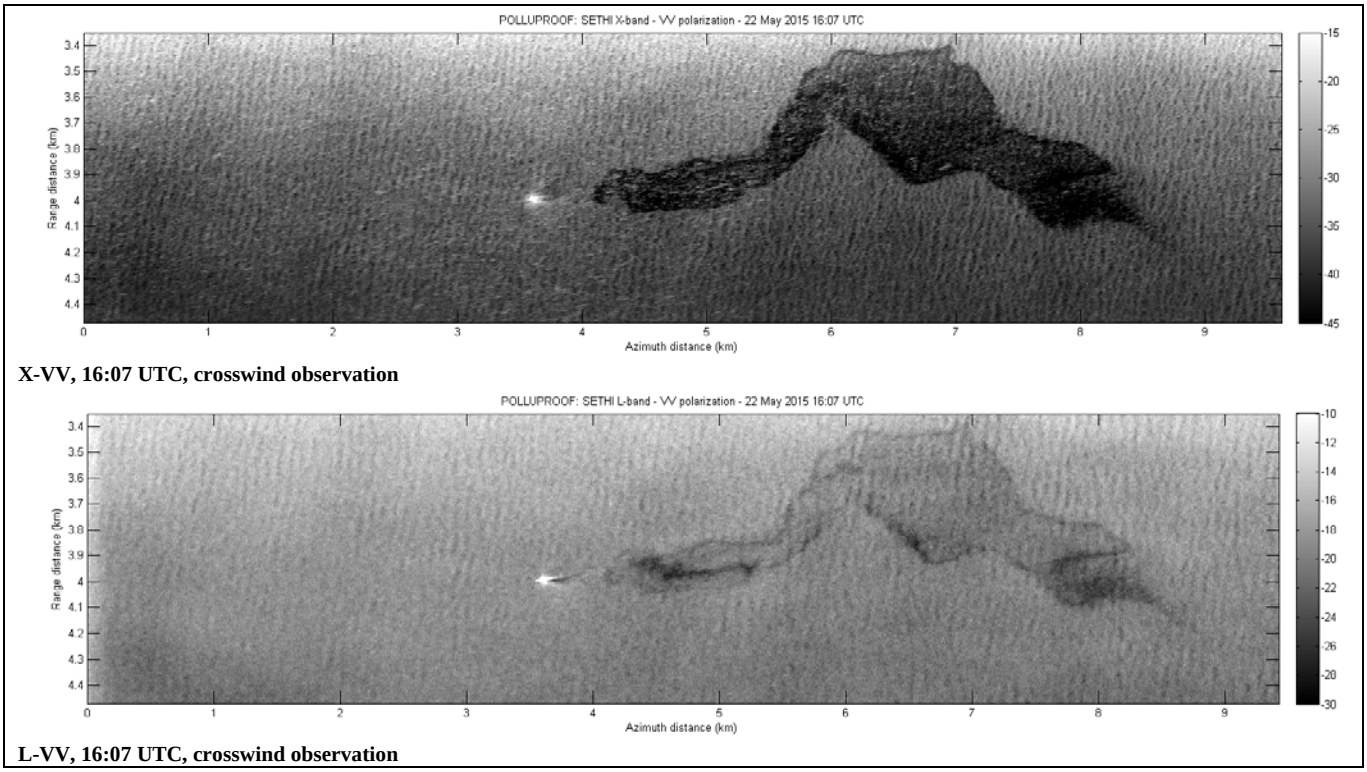

Figure 7 SAR images over rapeseed oil and FAME - X-VV (top) and L-VV (bottom) - 16:07 UTC.

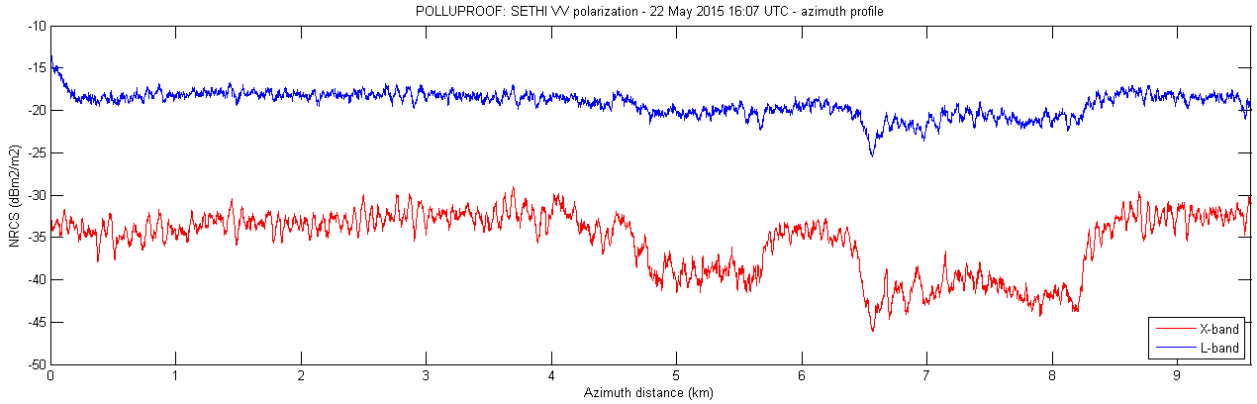

Figure 8 Range profile at X-band (red) and L-band (blue).

4.2 Detection and Quantification of Impact on the Ocean Surface

As presented in paragraph 3.2, the *Normalized Polarization Difference (NPD)* can be used for detection of HNS at sea and quantification of their impact on the ocean surface.

The proposed method is divided into 2 steps: as the contrast between the spill and ocean clean surface is more pronounced at X-band than at L-band, a detection mask is first calculated by thresholding the NPD map at X-band. Then, since we observe more variation of the signal into the spill at L-band than at X-band, the detection mask is applied to the NPD map computed at L-band.

Results are presented below: Normalized Polarization Difference map at X- and L-band, thresholded for values greater than 0.7 at X-band, in the case of xylene (Figure 9) and FAME and rapeseed oil (Figure 10).

We can observe that, first the spill is well identified using this automatic method, then information provided by the two frequencies is effectively different. This observation is particularly conspicuous on the spill of the 3rd flight (FAME and rapeseed oil): at X-band values of NPD are almost always close to 1.0 (between 0.8 and 1.0); whereas at L-band much more fluctuations are observed. At X-band, response is saturated by the presence of the spill. This frequency is perfectly suited for detection but does not seem to provide information on the thickness. At lower frequency (L-band in our case), the EM signal backscattered by the slick fluctuates with the impact of the product on the sea surface. Hence, L-band can provide useful information for spill quantification and characterization.

Figure 11 shows two range profiles over xylene and FAME at X- and L-band. Clearly, NPD values at X-band are always ranging from 0.8 to 1.0, while the dynamic at L-band is greater. Over the FAME, NPD value at L-band reveals a stronger impact of the HNS on the sea surface in the center of the spill than at the extremities.

Information provided by Normalized Polarization Difference and simultaneous use of two frequency bands, allow us to detect HNS at sea and to quantify their impact on the ocean surface in terms of roughness. However, results shown Figure 10 do not enable us to distinguish between the two products that form the spill (rapeseed oil and FAME).

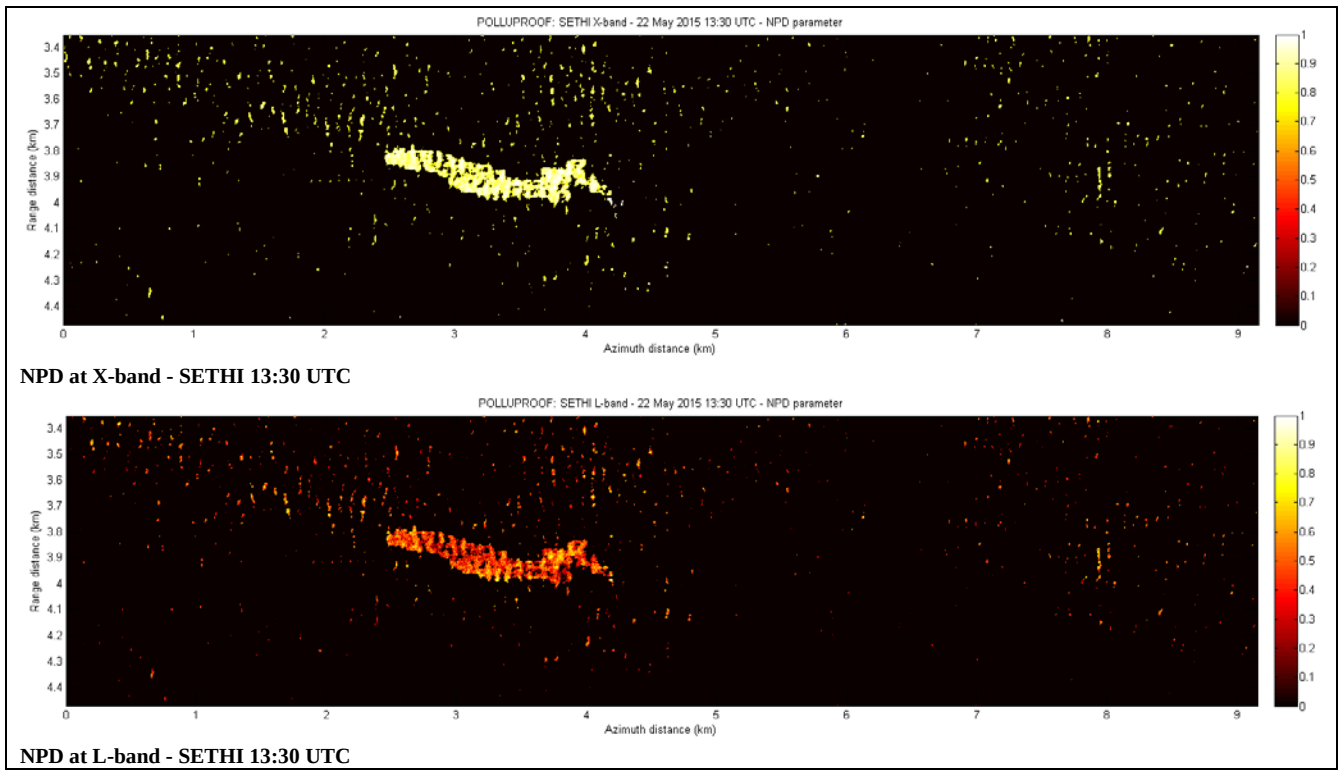

Figure 9 Normalized Polarization Difference (NPD) at X-band (up) and at L-band (down) - 13:30 UTC - xylene.

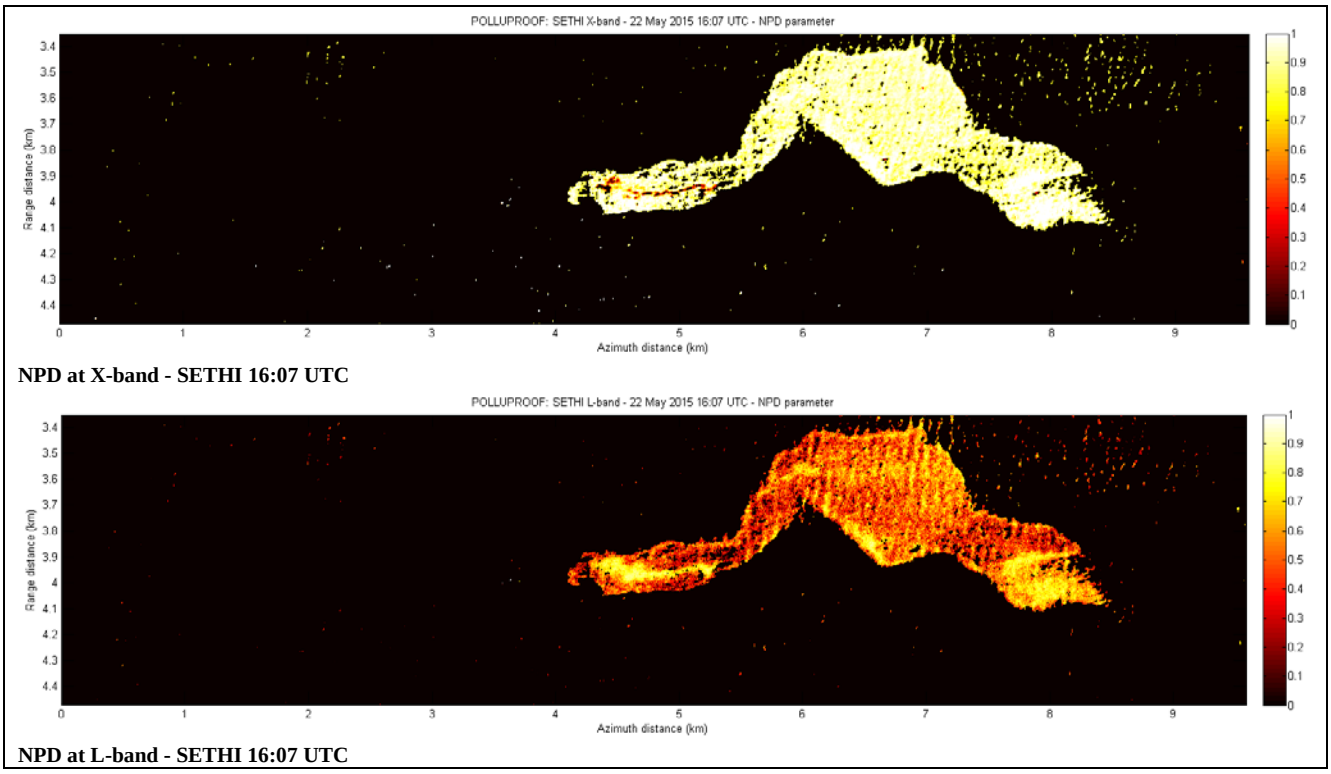

Figure 10 Normalized Polarization Difference (NPD) at X-band (up) and L-band (down) - 16:07 UTC - FAME and rapeseed oil.

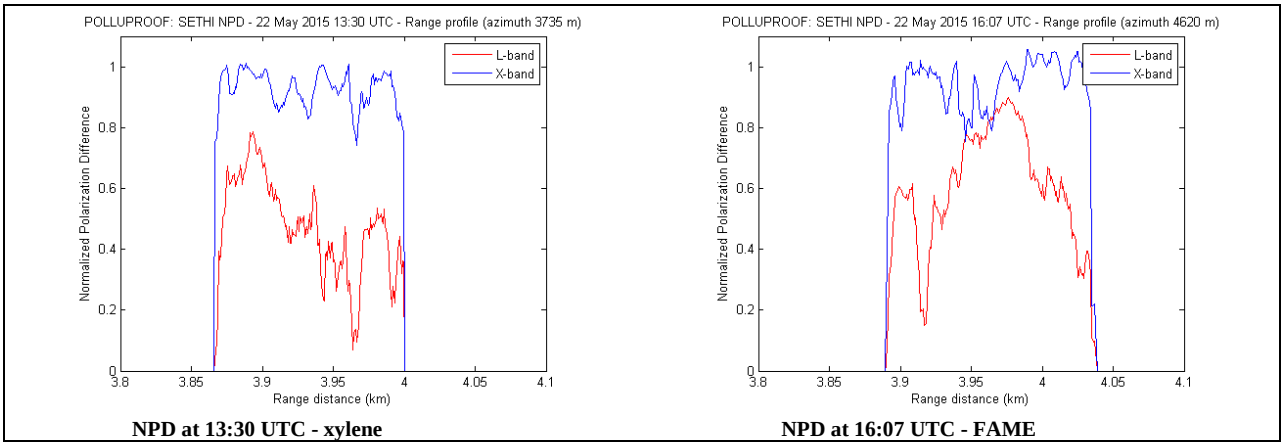

Figure 11 Normalized Polarization Difference (NPD) range profiles over xylene (left) and FAME (right) at X-band (blue) and L-band (red).

4.3 Characterization

In the third exercise, spill is composed by rapeseed oil and FAME. The right part is rapeseed oil and the left part is FAME; in the middle there is a mixture of two. One can expect different behavior of each product on the sea surface: rapeseed oil is supposed to remain above the surface and produce a more or less homogeneous film. FAME will form a cloud in the water column composed by micro-droplets. This is confirmed by observations made from the ship during the releases (Figure 12). These behaviors must be recovered by SAR imagery as they

impact the ocean surface in different ways: damping of capillarity waves and/or modification of the dielectric constant by mixing with sea water.

FAME: 3D plume / mix between HNS and water **Rapeseed oil**: discontinuous film on the surface

Figure12 Photos taken from the ship during the release of the FAME (left) and the rapeseed oil (right).

Following results presented in paragraph 4.2; we focus on L-band data and compute M_W, M_α and M_{dex} parameters using the method presented in paragraph 3.3 and initially published in (Minchew, 2012). As for Normalized Polarization Difference map (see 4.2), a detection map has been used beforehand and values have been computed for each pixel detected as HNS using X-band data.

Figure 13 shows maps obtained over the full region of interest: the normalized damping factor (M_W), the normalized power attenuation factor (M_α) and the mixing index (M_{dex}). We clearly observed the separation between the two products constituting the spill (see M_{dex} Figure 13).

Figure 14 shows histograms (NPD at X- and L-band, M_W, M_α and M_{dex}) over xylene, rapeseed oil and FAME. Xylene and rapeseed oil have similar responses: M_α is close to 0, M_{dex} is greater than 0 and M_W and NPD at L-band are equal; which corresponds to the presence of a film on the sea surface that damped the short waves. FAME has a different behavior: M_α is no longer negligible and thus M_{dex} is negative which means that, as expected, mixing is more present over FAME than over rapeseed oil and xylene. For the three products, NPD at X-band is always significantly high (greater than 0.9). Over the FAME, NPD at L-band allows us to distinguish two areas corresponding to two different concentrations, as it can be seen in Figure 10.

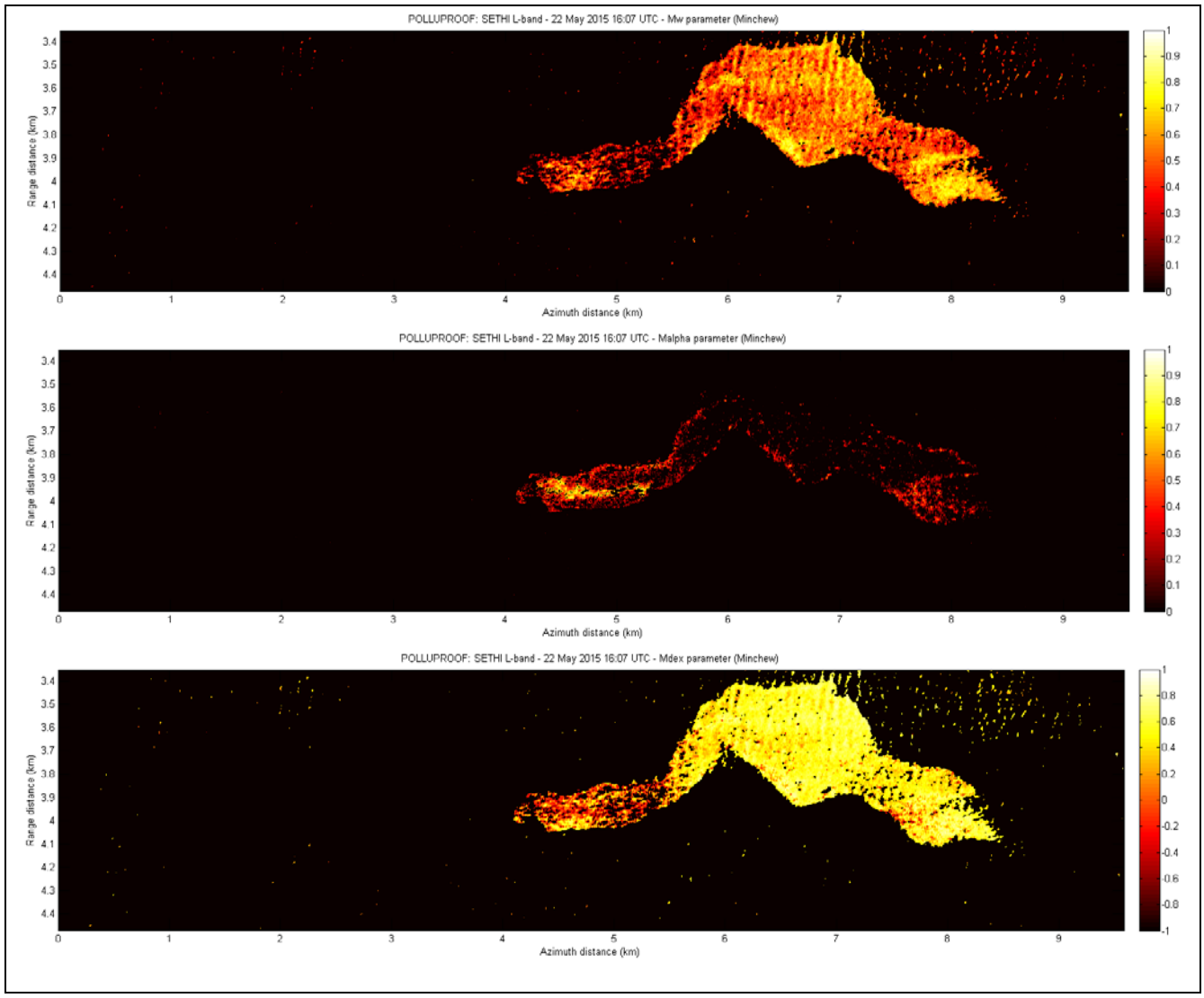

Figure 13 M_W (top), M_α (middle) and M_{dex} (bottom) - L-band SAR acquisitions at 16:07 UTC - FAME and rapeseed oil.

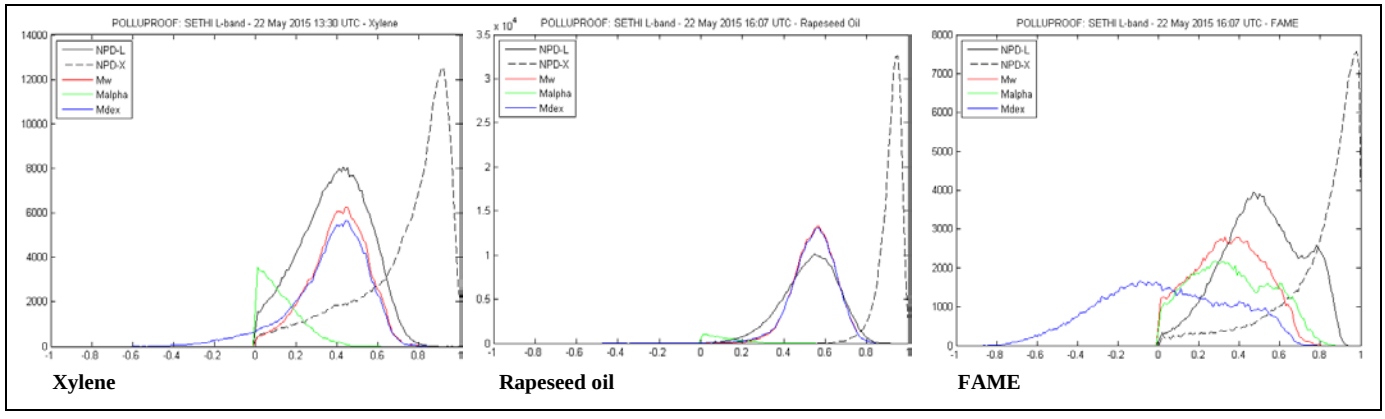

Figure 14 Histograms: NPD L-band (black), NPD X-band (dash black), M_W (red), M_α (green) and M_{dex} (blue) over xylene (left), rapeseed oil (center) and FAME (right).

5 Conclusion

Due to the increase of maritime transport of Hazardous and Noxious Substances (HNS), defined by the 2000 OPRC-HNS Protocol as substances other than hydrocarbon oil which, if introduced into the marine environment, is likely to create hazards to human health, controlling chemical pollution at sea becomes crucial. As for oil spill, remote sensing is of great interest for detecting, quantifying and characterizing chemical products that were discharged. However, our knowledge on the ability of remote sensing to achieve this is still limited.

An experimental campaign of acquisition (POLLUPROOF) has been conducted in May 2015 over the Mediterranean Sea during which controlled releases of hazardous and noxious substances have been realized; the aim being to establish a procedure for collecting evidence of illegal maritime pollution by noxious and hazardous liquid substances using airborne sensors.

Among the six products tested during this experimentation at sea, three have been detected without any ambiguity using SAR imagery: rapeseed oil, FAME and xylene. For the three others, the non-detectability can be caused either by a high volatility of tested products or by an impact into the water column that physically does not affect the backscattered signal at microwave frequency.

In addition, to demonstrate the ability of radar imagery to detect some HNS, two original results were presented in this paper: first an accurate method using X- and L-band radar imagery has been developed to detect and quantify the impact of chemical products at sea. X-band can easily detect the spills, even when the impact on the surface is limited; L-band is then used to quantify this impact. A *Normalized Polarization Difference* (NPD) parameter is then introduced for this purpose. We showed that, at L-band, the NPD parameter takes a wide range of values within the spill; this variation is related to the impact of the product on the ocean surface. Of course, this important result is only accessible to earth observation systems whose instrumental noise level is low enough. Then, we showed that the distinction between two HNS (with different thickness) within the same spill is possible with radar imagery only. We conclude that, using SAR data with the suitable wavelength can allow us to define the characteristics of the slick along a spectrum ranging from thin surface films to thicker emulsions. This information is critical for efficient cleanup operations.

As a future work, methods developed and tested on HNS will be tested on X- and L-band SAR data acquired by ONERA during the Norwegian oil spill experiment organized and managed by NOFO (Norwegian Clean Sea Association for Operating Companies) in June 2015.

6 Acknowledgments

Research presented in this paper is part of the POLLUPROOF research program (ANR-13-ECOT-007) funded by the French National Research Agency (ANR).
Authors are very grateful to everyone involved in the experiment at sea (ONERA - CEDRE - AVDEF - DGDDI - French Navy) and those who participated to SAR data processing. They are also very grateful to G. Soriano and C.-A. Guerin for GO-SSA modeling and to P. Dubois-Fernandez and H. Oriot from ONERA for successful discussions.

7 References

Angelliaume, S., P. Dubois-Fernandez, V. Miegebielle, and D. Dubucq, "Polarimetric parameters for oil slicks detection using SAR data remote sensing - An evaluation," in *Geoscience and Remote Sensing Symposium (IGARSS), 2015 IEEE International*, pp. 3794-3797, 2015.

Angelliaume, S., V. Fabbro, G. Soriano and C.-A. Guerin, "The GO-SSA Extended model for all-incidence sea clutter modeling", in *Geoscience and Remote Sensing Symposium (IGARSS), 2014 IEEE International*, pp. 5017-5020, 2014.

Bonin, G., P. Dubois-Fernandez, O. Ruault-du-Plessis, S. Angelliaume, H. Cantalloube, H. Oriot, and C. Coulombeix, "The new ONERA multispectral airborne SAR system in 2009", in *Radar Conference, 2009 IEEE*, pp. 1-3, 2009.

Brekke, C. and A.H.S. Solberg, "Oil spill detection by satellite remote sensing", *Remote Sensing of Environment*, ISSN 0034-4257, *95*(1): 1- 13, 2005.

Elfouhaily, T., B. Chapron, K. Katsaros, and D. Vandemark, "A unified directional spectrum for long and short wind-driven waves", *J. Geophys. Res*., 102(C7): 15 781–15 796, 1997.

Gade, M., W. Alpers, H. Hühnerfuss, H. Masuko and T. Kobayashi, "Imaging of biogenic and anthropogenic ocean surface films by the multifrequency/multipolarization SIR-C/X-SAR", *J. Geophys. Res.*, 103(C9): 18 851–18 866, 1998.

Garcia-Pineda, O., B. Zimmer, M. Howard, W. Pichel, X. Li, and I. MacDonald, "Using SAR images to delineate ocean oil slicks with a texture-classifying neural network algorithm (TCNNA)", *Can. J. Remote Sens.*, 35(5): 411–421, 2009.

Girard-Ardhuin, F., G. Mercier, F. Collard and R. Garello, "Operational oil-slick characterization by SAR imagery and synergistic data", *IEEE J. Ocean. Eng.*, 30(3): 487–495, 2005.

Gregers-Hansen, V. and R. Mittal, "An improved empirical model for radar sea clutter reflectivity*", IEEE Transaction on Aerospace and Electronic Systems*, 48(4): 3512–3524, 2012.

Guérin, C.-A., G. Soriano and B. Chapron, "The weighted curvature approximation in scattering from sea surfaces," in *Waves in Random and Complex Media*, 20(3):364–384, 2010.

Hajnsek, I., E. Pottier and S.R. Cloude, "Inversion of surface parameters from polarimetric SAR," in *IEEE Transactions on Geoscience and Remote Sensing*, 41(4): 727-744, 2003.

IMO, http://www.imo.org/en/OurWork/Safety/Cargoes/CargoesInBulk/Pages/IBC-Code.aspx

Leifer, I., W. Lehr, D. Simecek-Beatty, E. Bradley, R. Clark, P. Dennison, Y. Hu, S. Matheson, C. Jones, B. Holt, M. Reif, D. Roberts, J. Svejkovsky, G. Swayze, and J. Wozencraft, "State of the art satellite and airborne marine oil spill remote sensing: Application to the BP Deepwater Horizon oil spill", in *Remote Sensing of Environment*, 2012.

Minchew, B., *"*Determining the mixing of oil and sea water using polarimetric synthetic aperture radar*", in Geophys. Res. Lett.*, 39, L16607, 2012.

Minchew, B., C.E. Jones, and B. Holt, "Polarimetric Analysis of Backscatter from the Deepwater Horizon Oil Spill Using L-Band Synthetic Aperture Radar", in *IEEE Transactions on Geoscience and Remote Sensing*, 50(10): 3812-3830, 2012.

Kudryavtsev, V.N., B. Chapron, A.G. Myasoedov, F. Collard, and J.A. Johannessen, "On Dual Co-Polarized SAR Measurements of the Ocean Surface", in *Geoscience and Remote Sensing Letters, IEEE* , 10(4): 761-765, 2013.

Solberg, A.H.S., "Remote Sensing of Ocean Oil-Spill Pollution", in *Proceedings of the IEEE*, 100(10): 2931-2945, 2012.

Soriano, G. and C.-A. Guérin, "A Cutoff Invariant Two-Scale Model in Electromagnetic Scattering From Sea Surfaces", in *Geoscience and Remote Sensing Letters, IEEE*, 5(2): 199-203, 2008.

Valenzuela, G.R., "Theories for the interaction of electromagnetic and oceanic waves - A review," in *Boundary-Layer Meteorology*, 13(1-4): 61–85, 1978.

Wismann, V., M. Gade, W. Alpers, and H. Hühnerfuss, "Radar signatures of marine mineral oil spills measured by an airborne multi-frequency radar", in *Int. J. Remote Sens.*, 19(18): 3607–3623, 1998.